Available online at www.sciencedirect.com
SCIENCE DIRECT®
Journal of Sound and Vibration 285 (2005) 743–758
JOURNAL OF SOUND AND VIBRATION
www.elsevier.com/locate/jsvi

Short Communication

Vibration analysis and measurement of a gradient coil insert in a 4 T MRI

G.Z. Yao[a], Chris K. Mechefske[a,*], Brian K. Rutt[b]

[a]*Department of Mechanical Engineering, Queen's University, McLaughlin Hall, Kingston, Ontario, Canada K7L 3N6*
[b]*Imaging Research Laboratories, John P. Robarts Research Institute, London, Ontario, Canada N6A 5K8*

Received 5 January 2004; received in revised form 8 October 2004; accepted 24 October 2004
Available online 28 December 2004

Abstract

High speed switching of current in gradient coils within high magnetic field strength Magnetic Resonance Imaging (MRI) scanners may result in high acoustic sound pressure levels in and around these machines. Many studies have already been conducted to characterize the sound field in and around MRIs and various methods have been investigated to attenuate the noise generated. To characterize the vibration properties of the gradient coil, a modified Finite Element (FE) model was developed according to the dimensional design of an available gradient coil insert and the concentration of the copper windings in the coil. The finite element analysis results were verified through experimental modal testing of the same gradient coil in a free–free state (no boundary constraints). Comparisons show that the FE model predicts the vibration properties extremely accurately. Based on the verified FE model, boundary conditions (supports) were added to the model to simulate the operating condition when the gradient coil insert is in place in an MRI machine. Vibration analysis results from the FE model were again verified through experimental vibration testing with the gradient coil insert installed in a 4 T MRI and excited using swept sinusoidal time waveforms. Through a comparison of the vibration signals generated it was found that the vibration resonances, both from the FE model and the experimental vibration testing, shift to higher frequencies after the boundary constraints were applied, as was expected. The predicted vibration response was very close to that measured from the gradient coil insert in operation. The FE modeling procedure that has been developed could easily be used to accurately predict the vibration properties of other gradient

*Corresponding author. Tel.: +1 613 5333148; fax: +1 613 5336489.
E-mail address: chrism@me.queensu.ca (C.K. Mechefske).

0022-460X/$ - see front matter
doi:10.1016/j.jsv.2004.10.045

coil designs. Furthermore, the vibration analysis results from the FE model could be used in acoustic noise analysis to predict the sound pressure level produced by different types of input current pulse sequences.

1. Introduction

Ongoing development of magnetic resonance imaging (MRI) technology is resulting in even more powerful scanners, with high static magnetic field strength (7–8 T) and high gradient coil current switching speeds. These developments are driven by the desire to obtain higher quality images that reveal more detail of the internal structure of the biological subjects being examined. It is generally acknowledged that a serious limiting factor in the development of these machines is the acoustic noise that they generate during scanning [1]. The main source of this acoustic noise is the gradient coil, which is used to produce a spatially varying dynamic magnetic field inside the MRI bore [2]. The high acoustic noise generated by the gradient coil results in problems for patients and health care workers that range from simple annoyance to difficulties in verbal communication, heightened anxiety, temporary hearing loss and possible permanent hearing impairment for persons who are exposed to these noisy environments for long periods of time. The vibration of the gradient coil that generates the acoustic noise will also affect the image quality and resolution since the radio frequency receiver is often integrated into the gradient coil [3]. It is therefore important to find ways to reduce the vibration and acoustic noise levels of MRI scanners in order to improve both the image resolution and the patient and working environment in and around the scanners.

To create a gradient magnetic field during scanning a time varying current is applied to the gradient coil windings. In the presence of the high static magnetic field this generates a Lorentz force distribution that acts on the coil. This time varying force distribution results in vibration of the gradient coil during scanning. The forces that are normal to the surface of the coil generate movement of the coil surface and subsequently the acoustic noise within and nearby scanners. The investigation of MRI gradient coil associated acoustic noise was first conducted in the late 1980s [4]. These investigations investigated the acoustic noise generation mechanisms involved, measurement instrumentation that was best suited for work inside and nearby scanners, and different test procedures. Later, extensive studies were performed using various MRI scanners and different pulse sequences [3,5,6–8]. Acoustic noise levels ranging from 80 to 130 dBA were reported and found to depend on the scanner field strength and pulse sequence.

More recently, considerable effort has gone into the design of new "quiet" gradient coils, development of active noise cancellation (ANC) techniques, and passive noise isolation for use on MRI machines [9–13]. Finite element analysis (FEA) as well as vibro-acoustic computational methods have also been used to estimate the acoustic noise distribution of the gradient coil during scanning [14,15]. However, not all the models were verified through experimental testing. The objective of this paper is to show the experimentally validated vibration prediction results generated using an FE model of a gradient coil insert.

To predict the vibration, and subsequently the acoustic noise, generated by a gradient coil an understanding of the vibration properties of the gradient coil is essential. Not only the pulse

sequence employed to excite the gradient coil, but also the structure of the gradient coil and the supports will affect the gradient coil response [9]. If the primary frequency of the excitation pulse sequence falls at or close to a vibration resonance frequency of the gradient coil (dictated by the coil structure and supports), large vibration amplitudes will be induced, which will in turn result in high acoustic noise levels.

For the purposes of this work a gradient coil insert was designed and fabricated for vibration and acoustic noise testing and measurement. The design used was based on a gradient coil insert developed for scanning small animals. A computational (finite element) model was also developed based on the gradient coil insert design used. The exact structure of the gradient coil insert was not duplicated in the FE model due to the high degree of complexity that would be required to model all the individual conductors. Instead, the overall structure was modeled using concentric layers to represent the conductors, the cooling tubes and the epoxy resin that provided the structural integrity of the cylinder. Each layer was modeled with variable elastic modulus values and damping ratios in the axial direction in order to better simulate the different conductor densities at different locations in the coil.

A comprehensive investigation of the vibration properties of the coil insert was conducted using FEA and experimental testing. Using the experimentally verified FE model, boundary conditions were then added to the model to simulate the real constraints that are in place when the gradient coil insert is being used inside an MRI bore. By applying the known Lorentz force distribution, the vibration response was obtained with the FE model. Finally, an experimental vibration test was conducted using swept sinusoidal excitation to verify that the boundary conditions added to the FE model are accurate.

The results of this investigation clearly show that the dynamic behavior (vibration) of a gradient coil insert can be accurately modeled using a computational model. The vibration resonances obtained in this study can also be used to predict the acoustic noise that would be generated by a coil. A validated predictive tool, such as the one described here, would help gradient coil designers to predict the vibration and acoustic noise that would be generated by a given design in the design stage. A redesign and/or optimization of the coil, based on the computational results, could then be done to minimize the acoustic noise.

2. Materials and methods

The gradient coil insert under investigation has a length of 680 mm, an outer-diameter of 353 mm and a wall thickness of 56.5 mm. It was designed to be installed in a 1.5 T GE MRI or a 4 T Varian/Siemens MRI for scanning small animals. Fig. 1 shows the gradient coil inside a 1.5 T GE MRI. There are three layers of copper windings (referred to as X, Y, and Z coils) embedded in a cylindrical epoxy resin tube. To cool the gradient coil when it is in use, two layers of cooling tubes were incorporated into the design, which are positioned between the X and Y layers, and between the X and Z layers. When in use inside an MRI the coil is supported with a wood and aluminum frame (as shown in Fig. 1), which is fixed to the coil with screws at both ends. Cooling water is pumped into the cooling tubes to take away the heat produced by the electric current.

Fig. 1. The gradient coil installed in a 1.5 T GE MRI.

2.1. Finite element model of the gradient coil

To study the vibration properties of the gradient coil in operation a finite element model was created based on the design parameters of the gradient coil. SDRC I-DEAS software was used to develop a 3-D model for the coil and conduct the FEA. In the model there are three layers of elements that simulate the copper windings and another two layers of elements that simulate the cooling tubes. To produce the required dynamic magnetic field inside the gradient coil, the copper windings are not distributed evenly in the longitudinal (Z) direction. The density of the copper windings close to the isocenter is much higher than at other positions within the coil. In order to model the variable concentration of the copper windings each copper winding layer was divided into three sections and the corresponding material properties were assigned to each section based on the concentration of copper windings in that section. Dimensional data used in the FE model came from the original design specifications and was corroborated with physical measurements.

The FE model is shown in Fig. 2. There are a total of 29,120 elements and 31,920 nodes in the model. Material testing experiments were carried out to determine the Young's modulus and damping coefficient of the epoxy resin. The measured Young's modulus is 9.3E9 and the damping coefficient is 0.018 at room temperature. These material properties will change with temperature and frequency. Considering these factors will unduly complicate the model for FEA. In this study, we assume that the material properties remain constant in the frequency range of interest. For the sake of simplicity, and for the purpose of comparison with experimental modal testing, the modal analysis was performed for the coil in the free–free state first, which means there were no initial boundary conditions (supports) applied to the coil. The FE model was verified through experimental modal testing by comparing the modal frequencies and mode shapes. The FE model was then modified, by adding detail and changing the damping coefficients slightly, to bring the simulated results into closer agreement with the experimental results. After validation of the FE model, the boundary condition constraints were added to the model to find the vibration resonances when the coil is in a normal operating condition.

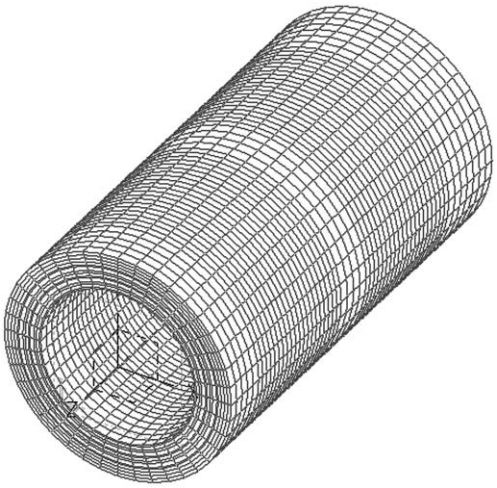

Fig. 2. FE model of the gradient coil.

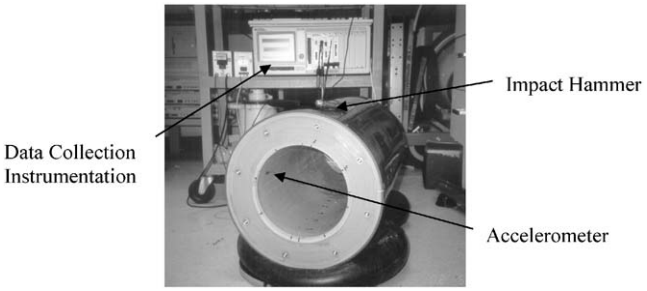

Fig. 3. Gradient coil used in modal testing.

2.2. Modal testing

Validation of the FE model is extremely important if it to be used as the basis for future design and testing. For the experimental modal analysis testing the gradient coil was assumed to exist in a free–free boundary condition state the same as that mentioned in the FE model analysis. The experimental testing was conducted with the gradient coil supported on low natural frequency air cushions in order to achieve the free–free boundary condition state. Natural frequencies and mode shapes of the coil in the frequency range of interest were then obtained through experimental testing and data analysis.

To accomplish the experimental modal testing and keep the same boundary conditions as those in the FE model, all cooling tubes, electric cables and the support frame were removed from the gradient coil before the experiment began. Fig. 3 shows the gradient coil used in modal testing. The coil was supported by two air cushions filled with low-pressure compressed air to simulate the free–free boundary condition experimentally. Acceleration measurements were taken on the inner surface of the coil at 22 equally spaced intervals in the longitudinal (Z) direction. At each measurement location there were 12 testing points distributed evenly around the inner surface of

the coil (every 30°). A total of 276 testing points were defined. An impact hammer was used to excite the gradient coil at a fixed position. Three accelerometers were attached to measure the acceleration response after excitation. All the signals from the accelerometers and the impact hammer were fed into a National Instruments (PXI-1020) data collection and analysis instrument.

The frequency response functions (FRF) were then obtained from the sampled data. The FRF at each sample point was calculated from an average of 5 measurements. All the calculated FRFs, including the definition of excitation point, the response points and the measurement directions were exported to the modal analysis software, ME'Scope. The ME'Scope software modeled the geometry of the gradient coil under test, linked it with the measured points and read the FRFs at each defined point. The modal frequencies and mode shapes of the gradient coil were then calculated using standard algorithms.

2.3. Finite element analysis of the gradient coil vibration during operation

To analyze the vibration of the gradient coil when the coil is seated in the static magnetic field of a scanner the FE model was used here again. A constraint condition was added to the FE model to simulate the real installation condition. To investigate the vibration properties of the gradient coil in the frequency range of interest, a swept sinusoidal wave from 100 to 3000 Hz was applied to the X-windings of the coil. The applied force distribution was then calculated based on the position of the windings in the static magnetic field, the applied electric current and the static magnetic field strength. The force distribution was then applied to the nodes of the FE model. The velocity response of the coil was then computed based on the applied excitation force.

2.4. Vibration measurement of the gradient coil during operation

To verify the FE model when used to predict vibration responses with the boundary conditions that represent normal operating conditions in place, vibration measurements will be conducted when the gradient coil was in operation with the same boundary constraints as used in the FE modeling. To measure the vibration of the gradient coil in operation in the MRI, the gradient coil insert with its wood and aluminum frame was laid on the patient bed in a 4 T Varian/Siemens whole body MRI machine. Due to the high static magnetic field present traditional accelerometers were considered unsuitable. A non-contact Laser Doppler Vibrometer (Polytec PI LDV-300) was used to measure the velocity of the gradient coil insert. To reduce the effect of the high static magnetic field strength on the electronic components in the laser head, measurements were taken with the laser head set as far as possible from the magnetic field (approximately 8 m from the isocentre in this case). A schematic diagram of the experimental setup is shown in Fig. 4.

To better show the experimental test rig, the main structure of the MRI and an acoustic liner installed in the MRI were not shown in Fig. 4. A special apparatus was designed with a reflecting mirror in order to direct the laser beam onto the inner surface of the gradient coil insert. The laser beam was aligned with the centerline of a plastic tube in which a reflecting mirror was installed at 45° to the laser beam. The laser beam was reflected onto the inner surface of the gradient coil via the mirror through a small slot cut on the tube. To reduce the vibration of the mirror, the tube was suspended from a rugged wooden frame structure, which was supported directly from the concrete floor without any direct contact with the patient bed or the main structure of the MRI.

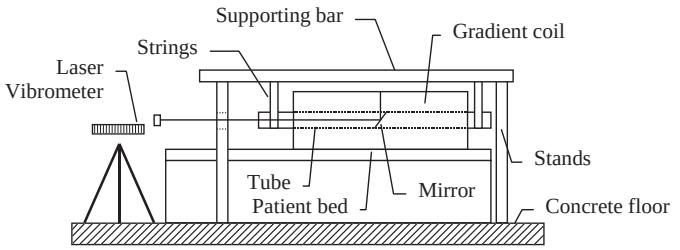

Fig. 4. Schematic diagram of the experimental testing rig.

The vibration measurement points were defined on the inner surface of the gradient coil insert by dividing the surface into 13 sections in the longitudinal (Z) direction and using 12 points on each circle (every 30°). A total of 168 measuring points were defined.

In the vibration testing a swept sinusoidal wave was used (100–3000 Hz every 60 s) to excite the insert. In order to match the FE modeling, the vibration testing used excitation to only one gradient coil (the X coil) without any current to the Y and Z coils. The excitation signal was programmed via the console and then output to the control system to be amplified prior to driving the coil. At the same time, the excitation signal was also exported to the PSV-300 system for recording and analysis. For each measuring point the PSV-300 system processes the excitation signal as well as the response signal. In order to determine the vibration resonances and the corresponding deflection shapes of the gradient coil insert under the swept sinusoidal excitation, FRFs of the response to the excitation were saved in files which can be processed by modal analysis software. To process the experimental measured FRFs the modal analysis software ME'scope was used here again. In ME'scope the structure of the gradient coil was created based on geometry of the structure and the location of measuring points. The same procedure was conducted as that described in Section 2.2 to obtain the vibration resonances and the corresponding deflection shapes in the frequency range of interest.

3. Results and discussions

3.1. Modal analysis

The modal analysis with the FE model was conducted in the frequency range from 1 to 3000 Hz. The rigid body modes are not considered here. Due to the symmetry of the gradient coil insert structure there are several symmetric modes. Symmetric mode shapes are those vibration modes that are related in shape (differing only in vibration direction) and occurring at only slightly different frequencies. Only one modal frequency from each set of symmetric modes is included in the results shown here.

A typical FRF from the experimental modal testing is shown in Fig. 5. It can be seen from this figure that the resonance frequencies are easy to distinguish across the entire frequency range of interest. One possible exception is in the frequency range from 1000 to 1200 Hz where there are several modes located close together on the frequency scale. However, these modes are of relatively low response amplitude suggesting a reduced significance. From the experimental results

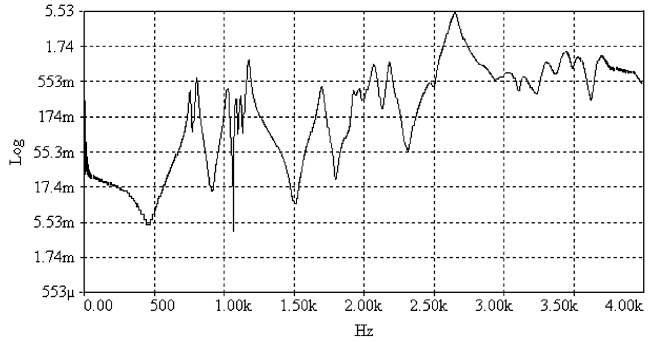

Fig. 5. A typical FRF from experimental modal testing.

Table 1
Modal frequencies and deviation between FE analysis and experimental modal testing

Mode	Modal testing results	FE model results	Deviation (%)
1	753	745	−1.0
2	793	805	1.4
3	1067	1178	9.4
4	1129	1193	5.3
5	1160	1235	6.0
6	1259	1240	−1.5
7	1909	1892	−0.9
8	1952	1978	1.3
9	1688	1983	14.8
10	2170	2232	2.7
11	2063	2381	13.3
12	2403	2579	6.8
13	2473	Not found	Not available
14	2630	2660	1.1
15	2924	3070	4.7

it was found that the first mode is around 750 Hz and there are 15 modes for the gradient coil insert in the frequency range of interest.

The modal frequencies and mode shapes in the frequency range from 1 to 3000 Hz were also obtained from FE analysis. Table 1 lists the modal frequencies from the FE analysis and the experimental modal testing for comparison purposes. By comparing the corresponding modes from the FE modal analysis and the experimental modal testing it is seen that there is only one resonance frequency seen in the FE analysis that was not detected using experimental modal testing. In general the results show that the FE model and the experimental measurements are in close agreement. The average deviation between the two methods is less than 5 percent. Since the experimental modal testing was conducted with excitation (hammer impacts) only in one direction, not all the vibration modes were necessarily excited. This is one possible explanation for the existence of fewer distinct modes in the experimental modal testing results than those found from the FE analysis.

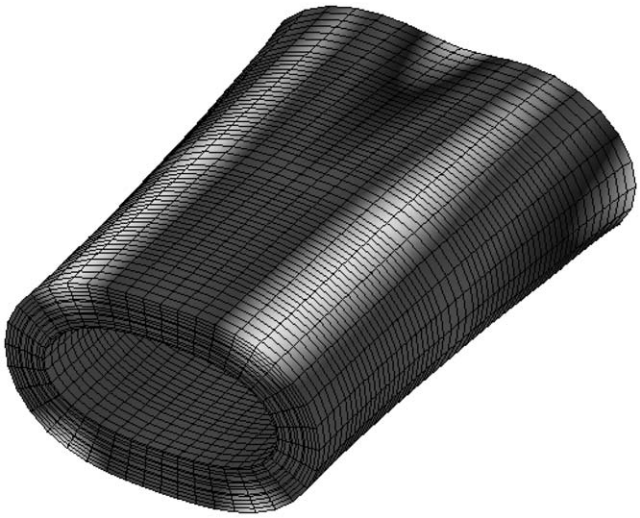

Fig. 6. 1st mode from FEA analysis (approximately 745 Hz).

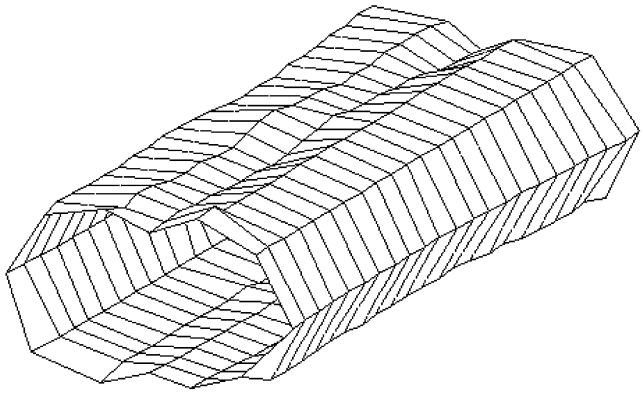

Fig. 7. 1st mode from experimental modal testing (approximately 753 Hz).

Figs. 6 and 7 depict the first mode shapes from the FE modal analysis and experimental modal testing respectively. As these figures show, the mode shapes are exactly the same. The only slight difference is that the predicted frequency is slightly smaller than that obtained from modal testing.

Figs. 8 and 9 show a comparison of mode shapes at a higher frequency for both the FE modal analysis and experimental modal testing. These two figures clearly show that the whole coil has a triangular shape in the cross-section with larger deflections at one end. The predicted modal frequency is again slightly smaller than that found in the modal testing.

Figs. 10 and 11 show the mode shapes from the highest frequency of interest in this study. Again they show the same shape for the FE modal analysis and experimental modal analysis with only a slight difference in the frequency.

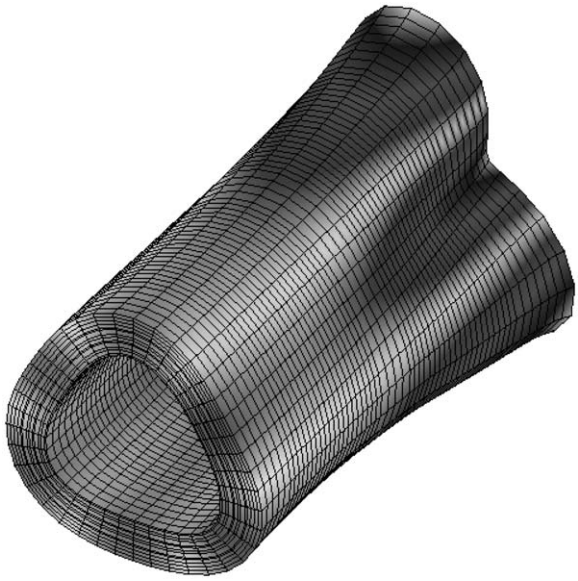

Fig. 8. Mode shape from FE analysis (approximately 1892 Hz).

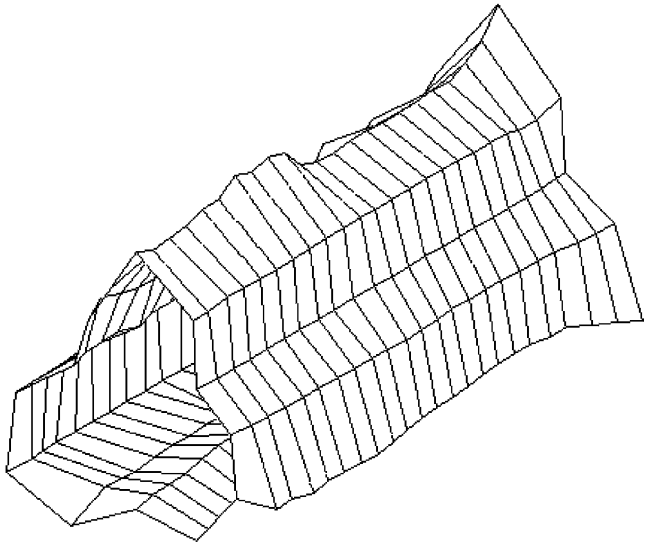

Fig. 9. Mode shape from experimental modal testing (approximately 1909 Hz).

From this comparison of the corresponding mode shapes and modal frequencies from the FE model and the experimental modal testing it is clear that the FE model is accurate and can be used to predict the modal frequencies and mode shapes of the coil insert in the frequency range of interest.

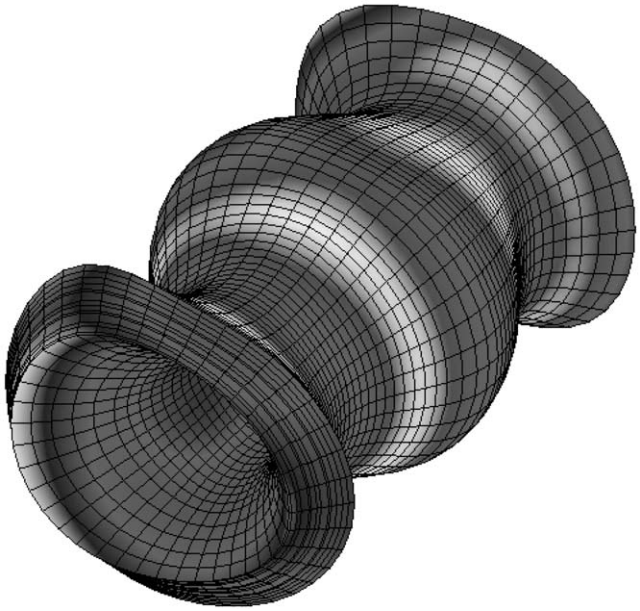

Fig. 10. Mode shape from FE analysis (approximately 3070 Hz).

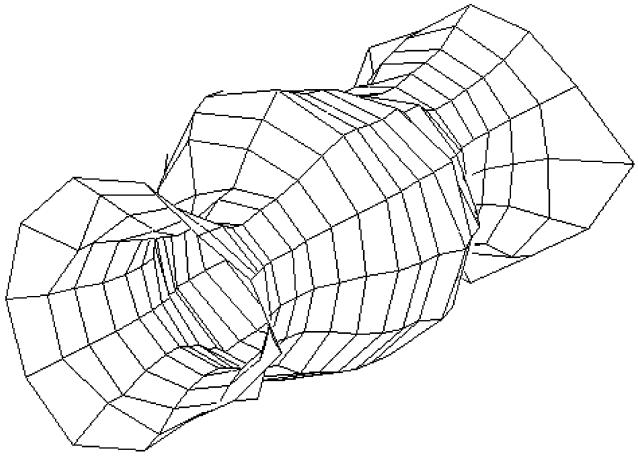

Fig. 11. Mode shape from experimental modal testing (approximately 2924 Hz).

3.2. Vibration analysis (coil insert inside MRI)

With the FE model now validated based on experimental testing results, new boundary conditions were added and the corresponding modal frequencies and mode shapes were again obtained. To compare the change of resonance frequency with respect to the change in boundary conditions, Table 2 lists some frequencies generated by the FE model in the free–free state and

Table 2
List of resonance frequencies from the FE analysis in free-free state and with the new boundary conditions

Mode	Frequency in free-free state (Hz)	Frequency with boundary constraints (Hz)
1	745	808
2	805	979
3	1178	1324
4	1193	1632
5	1235	1459
6	1240	1549
7	1892	1948
8	1978	2044
9	1983	2067
10	2232	2297
11	2381	2454
12	3070	3127

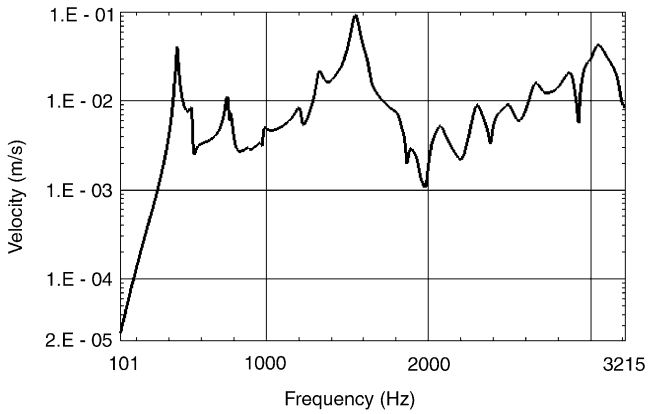

Fig. 12. Velocity response for a point on the inner surface of the gradient coil from FE model based vibration analysis.

with the new boundary conditions. As expected, all the corresponding frequencies from the FE modal analysis are shifted higher with the change in boundary conditions.

The Lorentz force distribution map was then applied to the FE model to compute the velocity response under the swept sinusoidal waves from 100 to 3200 Hz with the new boundary constraints in place. This simulates the real operational conditions that exist in an MRI. Only the Lorentz force distribution for X coil excitation were applied since only the X coil would be excited in the vibration measurement experiment. Fig. 12 shows a typical velocity response from the FE model based vibration analysis. The figure clearly indicates that there are several vibration resonances in the frequency range of interest. The corresponding vibration deflection shapes at the certain vibration resonance frequencies were also obtained. To clearly show the vibration deflection shapes of the gradient coil insert when in operation, the experimental FRF functions were used to obtain the vibration resonances as well as measured vibration deflection shapes. A typical FRF function from experimental vibration measurement is shown in Fig. 13.

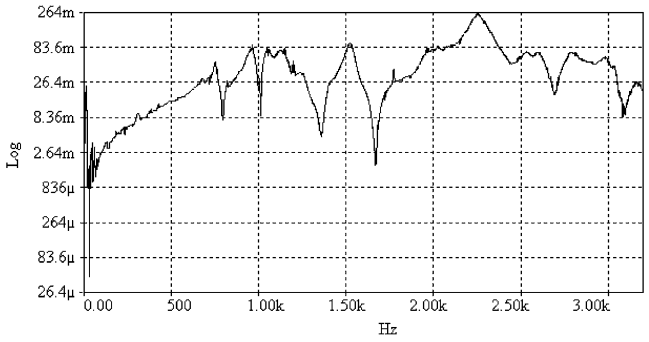

Fig. 13. A typical FRF response curve from vibration measurement.

Since the Lorentz force distribution was applied to the X coil only, the results from the FE model based vibration analysis and the experimental vibration measurement show that the main deflection of the gradient coil is in the X direction. It is also seen that the vibration deflection shapes at the resonance frequencies are a combination of the forced deflection in the dominant direction (the X direction) and the mode shape at that frequency. Figs. 14 and 15 show the vibration deflection shapes of the gradient coil both from the FE model based vibration analysis and the experimental vibration measurements. It is shown that the vibration deflection shapes at the resonance frequencies are the same, but the resonance frequency from the FE model based vibration analysis is over-estimated. This is probably caused by the addition of the boundary constraint in the FE model. The FE model constraint is applied at an exact point and absolutely no motion is permitted (infinite stiffness). In the experimental situation the gradient coil is laid on the patient bed and supported by a wood and aluminum frame (with finite stiffness). This kind of boundary condition is difficult to simulate in the FE model without incorporating the supporting structure into the model. This slight difference of boundary conditions between the FE model and the experimental conditions were found to mostly affect the vibration resonances predicted in the lower frequency range.

Figs. 16 and 17 show the vibration deflection shapes of the gradient coil insert at the same vibration resonance frequency. These two figures clearly indicate that the vibration deflection shapes are exactly the same as well as being very close in frequency. It is also clear from Fig. 16 that the boundary constraints used in the FE model produce local regions of high stress and zero deflection. This is an inaccuracy that will be corrected in the near future by incorporating the coil support frame into the model.

From the comparison of the vibration resonances and the vibration deflection shapes, both from the FE model based vibration analysis and the experimental vibration measurements, it is noted that the vibration resonance frequencies shift to higher frequencies when the coil insert boundary constraints are applied. It is also noted that the vibration deflection shapes are primarily in the same direction as the applied force distribution and are combined with the resonance frequency mode shapes. These results also prove that the FE model with boundary constraints is a very good tool for the simulation of gradient coil insert deflection during operation.

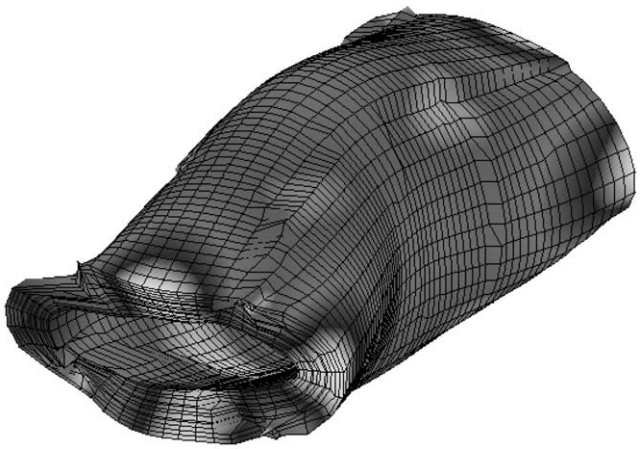

Fig. 14. Vibration deflection shape from FE model based vibration analysis (approximately 1324 Hz).

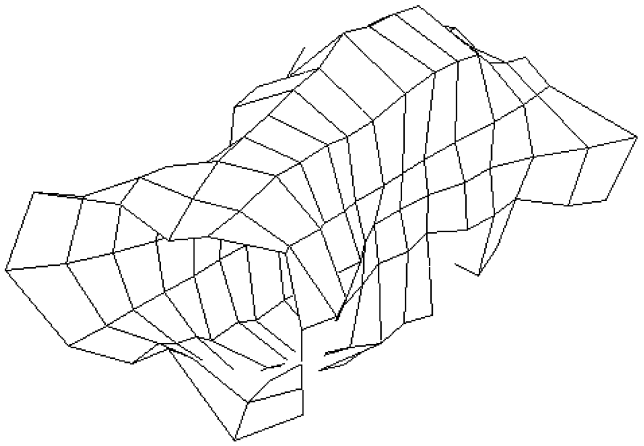

Fig. 15. Vibration deflection shape from experimental vibration measurement (approximately 1022 Hz).

4. Conclusions

An FE model of a gradient coil insert was developed based on the concept that, while the physical dimensions of the coil are symmetrical, the internal structure (concentration of the copper windings as a function of position) of the coil dictates that the model have variable stiffness along its length. Modal analysis was conducted to obtain the natural vibration frequencies and mode shapes of the gradient coil in a free–free state. To verify the FE model, experimental modal testing was performed under the same conditions. The results obtained from the comparison of the FE model based modal frequencies and the experimental mode shapes showed very close agreement.

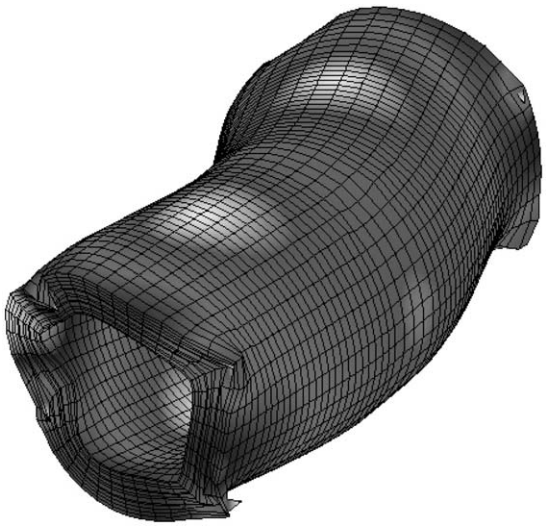

Fig. 16. Vibration deflection shape from FE model based vibration analysis (approximately 1549 Hz).

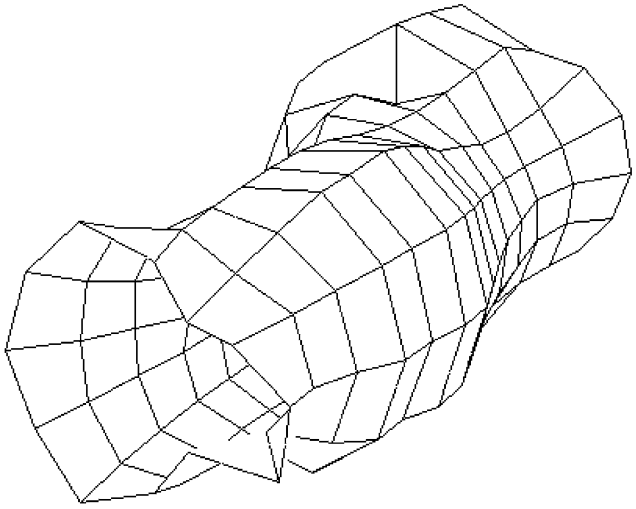

Fig. 17. Vibration deflection shape from experimental vibration measurement (approximately 1526 Hz).

Boundary constraints were then added to the FE model to simulate the gradient coil in a normal operational condition. The vibration response was then calculated using the Lorentz force distribution (swept sinusoidal excitation) on the X coil. Again, to verify the FE model, experimental vibration measurements were conducted when the gradient coil was in a normal operational condition and driven the same type of excitation input as used for the FE model. A comparison of the vibration resonance frequencies showed that the vibration resonances were shifted to higher frequencies, as expected. The predicted vibration response was very close to that measured from the gradient coil during operation.

The validation of the FE model with operational boundary conditions will allow the prediction of the vibration of the gradient coil under other types of excitation. The response could also be used to predict the acoustic noise distribution in the coil when a working pulse sequence is applied to the coil. The prediction of acoustic noise distribution will be reported in a separated paper.

Acknowledgments

The authors wish to offer special thanks to Carl Gazdzinski and Andrew Alejski at Robarts Research Institute, London, Ontario, Canada for their kind help in providing the structural dimensions of the gradient coil insert and setting up the modal testing and the vibration measurement experiments. This work was funded through an NSERC-CIHR Collaborative Health Research Project grant (227285-99 CHRPJ) and an Ontario Research and Development Challenge Fund grant.

References

[1] B.K. Rutt, Safety issues in MRI, *The 11th Scientific Meeting of the International Society for Magnetic Resonance in Medicine*, Toronto, Canada, July 2003, Plenary Address.
[2] C.K. Mechefske, R. Geris, J.S. Gati, B.K. Rutt, Acoustic noise reduction in a 4 T MRI scanner, *Magnetic Resonance Materials in Physics, Biology and Medicine* 13 (2002) 172–176.
[3] Y. Wu, B.A. Chronik, C. Bowen, C.K. Mechefske, B.K. Rutt, Gradient-induced acoustic and magnetic field fluctuation in a 4 T whole-body MR imager, *Magnetic Resonance in Medicine* 44 (2000) 532–536.
[4] R. Hurwitz, S.R. Lane, R.A. Bell, M.N. Brant-Zawadzki, Acoustic analysis of gradient-coil noise in MR imaging, *Radiology* 173 (1989) 545–548.
[5] F.G. Shellock, S.M. Morisoli, M. Ziarati, Measurement of acoustic noise during MR imaging: evaluation of six "worst-case" pulse sequences, *Radiology* 191 (1994) 91–93.
[6] M.J. McJury, Acoustic noise levels generated during high field MR imaging, *Clinical Radiology* 50 (1995) 331–334.
[7] S.A. Counter, A. Olofsson, G. Grahn, E. Borg, MRI acoustic noise, sound pressure and frequency analysis, *Magnetic Resonance Imaging* 7 (1997) 606–611.
[8] D.L. Price, J.P. DeWilde, A.M. Papadaki, J.S. Curran, R.I. Kitney, Investigation of acoustic noise on 15 MRI scanners from 0.2 T to 3 T, *Magnetic Resonance Imaging* (2001) 288–293.
[9] Z.H. Cho, S.T. Chung, J.Y. Chung, A new silent magnetic resonance imaging using a rotating DC gradient, *Magnetic Resonance in Medicine* 39 (1998) 317–321.
[10] C.K. Chen, T.D. Chiueh, J.H. Chen, Active cancellation systems of acoustic noise in MR imaging, *IEEE Transactions on Biomedical Engineering* 46 (1999) 186–199.
[11] W.A. Edelstein, R.A. Hedeen, R.P. Mallozzi, S.A. El-Hamamsy, R.A. Ackermann, T.J. Havens, Making MRI Quieter, *Magnetic Resonance Imaging* 20 (2002) 155–163.
[12] P. Mansfield, B. Haywood, R. Coxon, Active Acoustic Control in Gradient Coils for MRI, *Magnetic Resonance in Medicine* 46 (2001) 807–818.
[13] C.K. Mechefske, Y. Wu, B.K. Rutt, MRI gradient coil cylinder sound field simulation and measurement, *Journal of Biomedical Engineering* 124 (2002) 450–455.
[14] C.K. Mechefske, Y. Wu, B.K. Rutt, Characterization of acoustic noise and magnetic field fluctuations in a 4 T whole-body MRI scanner, *Mechanical Systems and Signal Processing* 16 (2002) 459–473.
[15] J.X. Ling, W. Amor, G. DeMeester, Numerical and experimental studies of the vibration and acoustic behaviors of MRI gradient tube, *Proceedings of the Acoustics, Vibrations and Rotating Machines*, DE-vol. 84-1, ASME, 1995, pp. 311–317.